Halide anion effects and magnetostructural relationships in Iron(III) spin crossover complexes

Theerapoom Boonprab, Warisa Thammasangwan, Guillaume Chastanet, Mathieu Gonidec, Phimphaka Harding, David J Harding

CRYSTAL GROWTH & DESIGN

pubs.acs.org/crystal

Article

Halide Anion Effects and Magnetostructural Relationships in Iron(III) Spin Crossover Complexes

Published as part of Crystal Growth & Design special issue "Frontiers of Molecular Magnetism".

Theerapoom Boonprab,‖ Warisa Thammasangwan,‖ Guillaume Chastanet, Mathieu Gonidec, Phimphaka Harding,* and David J. Harding*

Cite This: *Cryst. Growth Des.* 2024, 24, 8145−8152

Read Online

ACCESS | Metrics & More | Article Recommendations | Supporting Information

ABSTRACT: A series of three compounds $[Fe(salEen\text{-}5\text{-}I)_2]Cl$ **1**, $[Fe(salEen\text{-}5\text{-}I)_2]Br$ **2**, and $[Fe(salEen\text{-}5\text{-}I)_2]I$ **3** in which salEen-5-I = 2-{[(2-(ethylamino)ethyl]imino)methyl}-4-iodophenolate is reported. Magnetic studies reveal that **2** exhibits an abrupt 2-step spin crossover close to room temperature around 288 K, while **1** and **3** exhibit gradual incomplete spin crossover spanning over 200 K. The use of structural parameters **A**−**C** to describe the nearest and next nearest neighbor contacts allows us to rationalize not only the abruptness of the spin crossover but also the stepped nature of the spin crossover in **2**. Comparisons with previously reported $[Fe(salEen\text{-}5\text{-}Br)_2]ClO_4$ and $[Fe(salEen\text{-}5\text{-}I)_2]ClO_4$ reveal that this magnetostructural relationship is applicable to a wider range of members of this family of complexes.

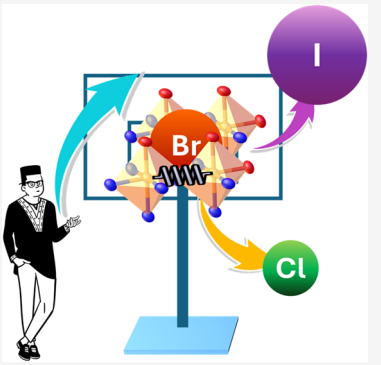

INTRODUCTION

Spin crossover (SCO) materials can interchange between low spin (LS) and high spin (HS) states, relying on a d^4−d^7 metal center exposed to changes in temperature, pressure, or light irradiation.[1,2] Spin crossover is accompanied by changes in the material properties, including, color, magnetism, and dielectric constants.[2] Octahedral complexes are typically used in SCO research with Mn(III),[3−5] Fe(II),[6,7] Fe(III),[8−11] and Co(II)[12,13] all widely explored. Among these systems, Fe(III) complexes are often air-stable, exhibit good magnetic performance, and have been successfully employed in devices.[14,15] In the case of Fe(III), the most common coordination sphere is an N_4O_2 donor set.[16−18] While this can be achieved with a hexadentate ligand, the use of two tridentate ligands such as Hqsal-X,[16,19−21] Hthsa-X[22−28] and Hsal-R-en-X[29−32] {Hqsal-X = X-2-[(8-quinolylimino)methyl]phenol, Hthsa = 2-(2-hydroxybenzylidene)hydrazine-1-carbothioamide and Hsal-*R*-en = 2-{[(2-(*R*-amino)ethyl)imino]methyl}phenol} is more common. The reason is that these ligands can be easily modified and permit control over the supramolecular contacts in the solid state, which is critical for the magnetic performance of SCO compounds.

Of particular relevance to the current work is the Hsal-R-en-X ligand class.[33−35] With these ligands, abrupt SCO in $[Fe(salEen\text{-}3\text{-}OMe)_2]PF_6$,[36,37] SCO with 8 K hysteresis in $[Fe(salEen\text{-}4\text{-}OMe)_2]NO_3$,[30] or near room temperature spin crossover in $[Fe(salEen\text{-}3,5\text{-}Br_2)_2]BPh_4$ have been reported.[31] Large structural contraction upon SCO has been reported in $[Fe(salEen\text{-}4\text{-}Br)_2]ClO_4$ and $[Fe(salEen\text{-}5\text{-}I)_2]ClO_4$, resulting in thermosalient properties.[38−40] These reports demonstrate the effect of the halide substituents, but the effect of the anion is still largely unexplored. In this report, we systematically explore $[Fe(salEen\text{-}5\text{-}I)_2]$halide including, Cl **1**, Br **2**, and I **3** and establish the key structural parameters which are able to rationalize the magnetic behavior of these compounds.

RESULTS AND DISCUSSION

Synthesis and Characterization. The ligand HsalEen-5-I was prepared (see Supporting Information (SI)) and used in situ following the reported synthesis of HnaphEen and HnaphBzen.[41,42] The synthesis of $[Fe(salEen\text{-}5\text{-}I)_2]Cl$ **1** and $[Fe(salEen\text{-}5\text{-}I)_2]Br$ **2** was carried out by reacting the ligand with the corresponding Fe(III) salt in the presence of a base in ethanol (Scheme 1). The resulting blue solid was further purified by recrystallization from CH_2Cl_2/hexane to give **1** and **2** as black crystals. Synthesis of **3** was achieved by postcomplexation anionic exchange from the nitrate complex (Scheme 1), followed by recrystallization to yield the product as black crystals. All the complexes were characterized by

Received: July 31, 2024
Revised: September 13, 2024
Accepted: September 16, 2024
Published: September 21, 2024

Scheme 1. Synthesis of [Fe(salEen-5-I)$_2$] Halide 1−3

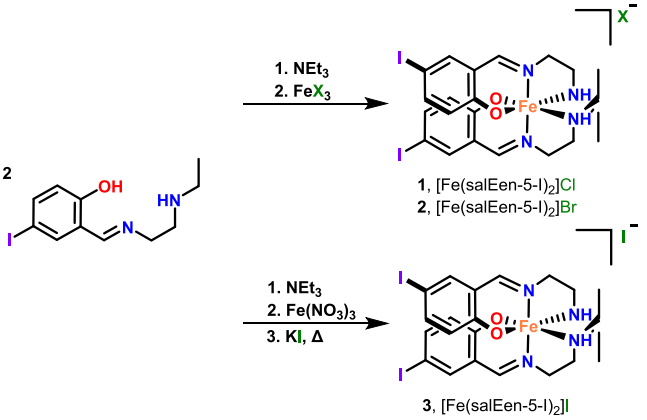

infrared (IR) and ultraviolet (UV)−visible spectroscopy, mass spectrometry, and elemental analysis (see SI).

IR spectroscopy of **1**−**3** (Table S1 and Figure S1) shows peaks corresponding to the amino group, aromatic rings, aliphatic backbone, and coordinating imine. The imine stretch is observed between 1616 and 1629 cm^{-1}. This is lower than the value of 1632 cm^{-1} reported in [Fe(salEen-5-I)$_2$]ClO$_4$,[39] especially in the case of chloride **1**. The values are found to increase as the size of the anion becomes larger; reflecting the ability of each anion to form a N−H···anion interaction, which affects the strength of the imine bond *via* the Fe center. The absorption spectra of each complex (Figure S2) in dichloromethane (CH_2Cl_2) exhibit a broad peak corresponding to the $\pi-\pi^*$ transition and the LMCT band. The presence of LMCT bands at approximately 590 and 670 nm matches the reported value for [Fe(salEen-5-I)$_2$]ClO$_4$,[39] [Fe(salEen-5-Br)$_2$]ClO$_4$[38] and [Fe(salMeen-5-Br)$_2$]ClO$_4$.[43] The position of λ_{max} is also consistent with HS Fe(III) as found in a range of [Fe(salRen)$_2$]$^+$ and [Fe(naphRen)$_2$]$^+$ complexes, exemplified by [Fe(naphEen)$_2$]halide.[41,44] It is also interesting that, despite being identical cationic complexes, the distribution of the HS and LS states in solutions of **1**−**3** is not the same. The intensity of the peaks corresponding to the LS state is higher than the HS in **1** and **2**, while the trend is opposed in **3**. This is likely a result of the differing strengths of the N−H···anion interactions in the solution state which favors different spin states at the metal center.

Solid-State Structure. Suitable black crystals for single crystal X-ray diffraction (SCXRD) of **1**−**3** were prepared from the slow diffusion of CH_2Cl_2 to hexane. Compound **1** is difficult to crystallize with the samples generally microcrystalline in appearance. The complexes are isostructural crystallizing in orthorhombic *Pbcn* at all temperatures (see Table S2 for the full crystallographic details). The asymmetric unit contains one salEen-5-I ligand with the halide counteranion and Fe(III) center sitting in special positions with half-occupancy (Figure 1). Consequently, the coordination sphere is octahedral with two crystallographically identical salEen-5-I ligands meridionally disposed to one another. The anion is held in place by N−H···X interactions with distances ranging from 2.21 to almost 2.63 Å, and dependent on the size of the anion.

The structures of **1**−**3** were recorded at different temperatures (Table 1). At 150 K, the average Fe−O and Fe−N bond lengths in **1** are 1.928 and 2.164 Å, respectively, indicative of HS Fe(III). In contrast, at 123 K, the Fe−N/O bond lengths in **2** are typical of LS Fe(III). The unusual magnetic profile of **2** (*vide infra*) led us to record structures at 275, 280, 293, and 305 K. Between 123 and 275 K, there is only a small increase in the average Fe−N/O bond lengths suggesting that the Fe(III) center remains mostly LS. At 280 K, the Fe−ligand bonds continue to lengthen and are *ca.* 0.04 Å longer than at 123 K, suggesting that the Fe(III) center is now 30% HS. At 293 K, the Fe−N/O bonds reach 2.08 Å indicative of the full HS state. Further heating to 305 K shows minimal change, confirming that SCO is complete. This demonstrates that SCO occurs mostly over 13 K consistent with abrupt SCO. These conclusions are supported by the Σ and Θ parameters, which have been measured with OctaDist.[38,45,46] Meanwhile, the average Fe−O/N bond lengths in **3** increase gradually from 1.97 to 2.05 Å upon heating from 293 to 425 K; nevertheless, the value is still a little lower than that expected for a full HS state. This indicates an incomplete gradual SCO within the studied temperature range. Note that heating beyond 425 K led to loss of crystallinity and slow degradation of the compound.

Magnetic Studies. The magnetic profiles of **1**−**3** were evaluated by SQUID and VSM magnetometry and displayed as magnetic susceptibility ($\chi_M T$, cm^3 mol^{-1} K) versus temperature (K) plots in Figure 2. While SCXRD data suggest that **1** should remain in the HS state, at least down to 150 K, we observe a very gradual increase in susceptibility from 0.80 cm^3 K mol^{-1} at 10 K to 1.81 cm^3 K mol^{-1} at 300 K consistent with incomplete SCO from a mostly LS state. We synthesized the sample multiple times and observed the same profile each time. The powder XRD (PXRD) data are broad and, in the case of **1**, almost amorphous. We have been able to obtain a reasonable PXRD of **1** from an extremely fresh sample, but as noted above, this compound is hard to crystallize and most samples, on which all bulk measurements were done, are amorphous (Figure S7). We hypothesize that two phases exist in **1** with the HS phase, for which we have the crystal structure, being a minor phase. Despite repeated attempts picking multiple crystals, we have been unable to collect SCXRD data on this major phase, which appears to be much less crystalline than the

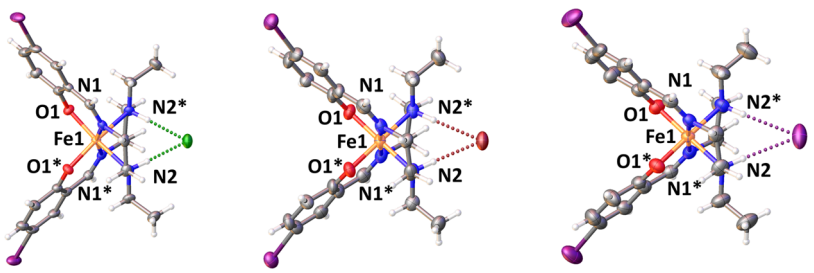

Figure 1. Coordination sphere of **1** (150 K), **2** (123 K), and **3** (293 K) viewed along the *a*-axis.

https://doi.org/10.1021/acs.cgd.4c01068
Cryst. Growth Des. 2024, 24, 8145−8152

Table 1. Selected Bond Lengths and Octahedral Distortion Parameters for $[Fe(salEen\text{-}5\text{-}I)_2]X$ Complexes Where X = Cl, 1, Br, 2 and I, 3

	1		2				3		
T (K)	150	123	275	280	293	305	293	400	425
Fe1−O_{ave} (Å)	1.928(3)	1.886(7)	1.878(4)	1.884(4)	1.913(13)	1.919(4)	1.877(3)	1.896(5)	1.904(5)
Fe1−N_{imine} (Å)	2.109(3)	1.933(8)	1.971(4)	1.987(4)	2.112(14)	2.088(4)	1.939(3)	2.052(4)	2.064(5)
Fe1−N_{amine} (Å)	2.219(3)	2.031(8)	2.080(4)	2.105(4)	2.210(13)	2.214(4)	2.061(3)	2.167(5)	2.182(5)
Fe1−N/O_{ave} (Å)	2.09	1.950	1.976	1.992	2.078	2.074	1.97	2.04	2.05
ΔFe−O/N (Å)			0.026	0.016	0.086	−0.004		0.07	0.01
Σ (deg)	66	34	36	39	55	61	36	49	53
Θ (deg)	264	99	120	135	229	240	109	191	208
ΔΣ, ΔΘ (deg)			2, 21	3, 15	16, 94	6, 11		13, 82	4, 17

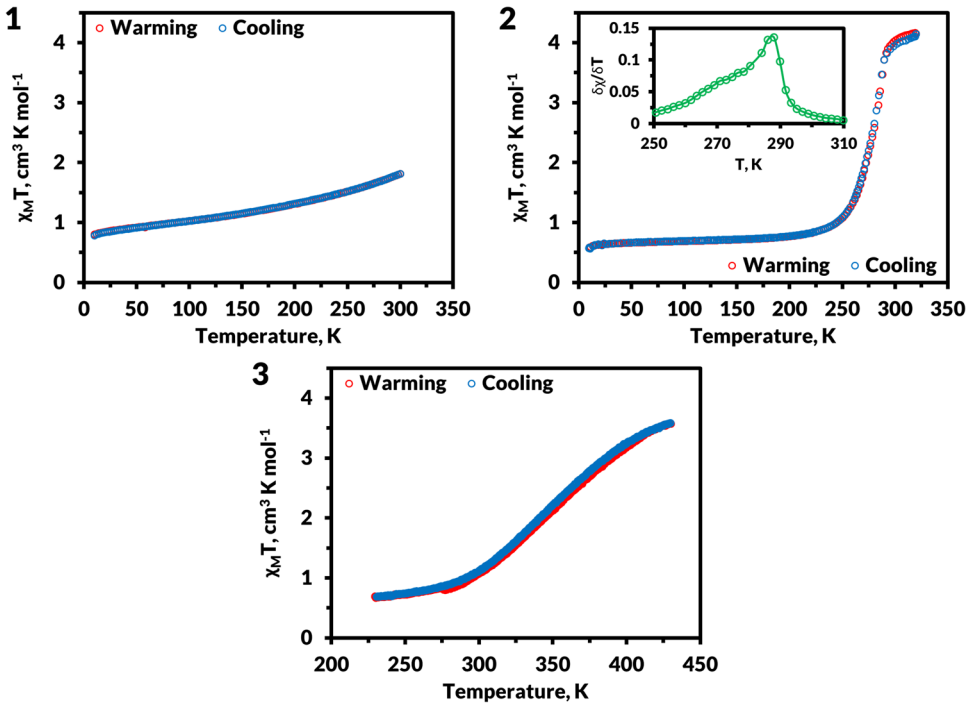

Figure 2. Solid-state magnetic susceptibility (cm^3 K mol^{-1}) against the temperature (K) of 1−3 and the first derivative plot of 2.

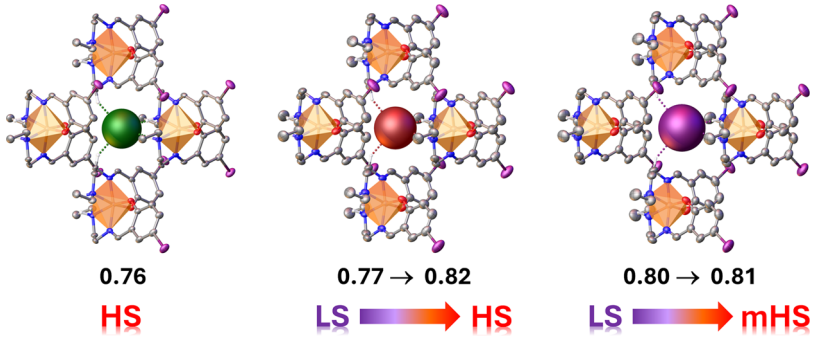

Figure 3. Spacefill packing of $[Fe(salEen\text{-}5\text{-}I)_2]$halide; 1 (left), 2 (center), and 3 (right) viewed along the c-axis in the HS state with the changes in the normalized N−H···anion contacts upon spin crossover.

orthorhombic phase discussed above. Such polymorphism and divergent magnetic behavior have also been observed in $[Fe(salEen\text{-}5\text{-}Br)_2]ClO_4$,[47] where the orthorhombic and monoclinic phases are accessible by altering the reaction temperature and hence the crystallization rate. We made similar attempts, but we are unable to separate the two phases in 1.

Compound 2 shows an increase in the magnetic susceptibility from 0.85 at 220 K to 4.73 cm^3 K mol^{-1} at 300 K, indicating complete SCO ($T_{1/2}$ at *ca.* 288 K). This agrees well with SCXRD results and reports of SCO active Fe(III) complex within the same ligand family.[38,39,48,49] However, a first derivative also reveals a small peak at 278 K, indicating that the SCO is stepped occurring over *ca.* 40 K. Repeated measurements on several different samples of 2

https://doi.org/10.1021/acs.cgd.4c01068
Cryst. Growth Des. 2024, 24, 8145−8152

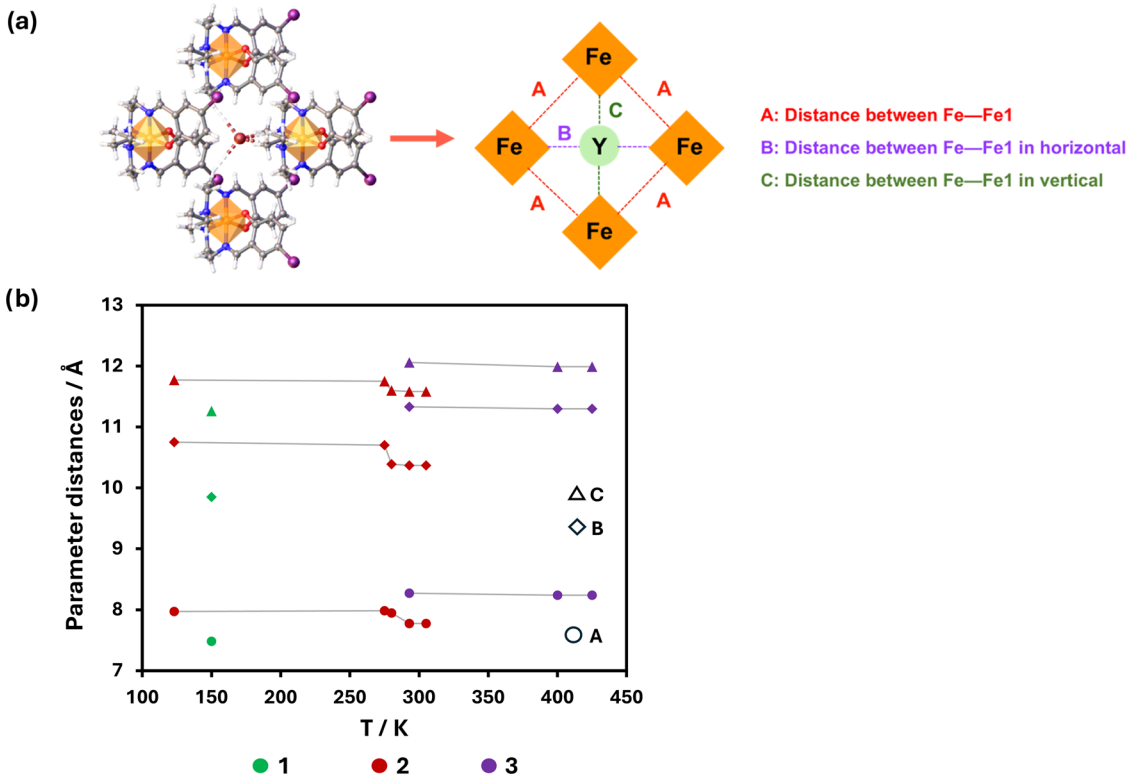

Figure 4. (a) Simplified illustration of $[Fe(salEen\text{-}5\text{-}I)_2]$halide **1**−**3** viewed along the *c*-axis showing the three structural parameters, **A**−**C** and (b) the trend in their values versus temperature.

reveal the same behavior confirming that the SCO is indeed stepped. In the case of **3**, $\chi_M T$ is 0.70 cm^3 K mol^{-1} at 230 K and indicative of LS Fe(III), while it is 3.50 cm^3 K mol^{-1} at 425 K. This value is a little lower than that reported in fully HS complexes[38,39,48,49] and consistent with the SCXRD data previously discussed. It follows that **3** exhibits a gradual and incomplete SCO from LS to mHS over this temperature range. It is also noteworthy that the $T_{1/2}$ values of these compounds increase as the anionic radii increase, indicating that larger anions stabilize the LS state. This is consistent with the [Fe(4-OH-sal-*N*-1,4,7,10)]halide family (4-OH-sal-*N*-1,4,7,10 = 1,8-bis(4-hydroxysalicylaldiminato)-3,6-diazaoctane) where $T_{1/2}$ increases from 275 to 375 K moving from chloride to iodide.[50] In contrast, $[Fe(atrz)_3](halide)_2$ (atrz = 4-amino-1,2,4-triazole) shows the opposite trend with the heavier halides exhibiting lower $T_{1/2}$ favoring the HS state,[51] indicating that the impact of the anion appears to be system specific.[52]

Magnetostructural Relationship. In an attempt to better understand the different SCO profiles of the compounds, we examined the packing in the structures. Note that we assume that the orthorhombic phase of **1** remains in the HS state, which is reasonable given that the magnetic studies suggest that even at low temperature a small fraction of the bulk material remains HS. This reveals that the packing in **1**−**3** is dominated by robust N−H···anion and C−H···anion interactions forming two-dimensional (2D) sheets in the *ab* plane (Figure 3). The normalized N−H···anion contacts are between 0.76 and 0.82 (Table S3), indicating strong interactions, with **1** being the strongest.[53,54] The values also increase gradually upon warming and do not appear to be related to SCO from LS to HS and level out throughout the period. The C−H··· anion contacts are clearly weaker with normalized contact values around 1.0 and, in contrast, become slightly stronger upon SCO from LS to HS. The aforementioned sheets then stack along the *c*-axis *via* weak C−H···π and C−H···I interactions indicating that the key contacts are primarily within the sheets.

To quantify the changes that occur due to SCO, three structural parameters, **A**−**C**, describing the square arrangement of the cationic complexes within the sheets around the anion have been defined (Figure 4a). First, it is clear that the parameters increase as the anion becomes larger, whatever the spin state, reflecting the space which is occupied in the lattice by the corresponding anions (Table 2). The small values observed for **1** suggest that there are minimum values of **A**−**C** beyond which SCO becomes impossible (Figure 4b). In the two SCO complexes, **2** and **3**, the values decrease with increasing temperature indicating that the anion becomes more tightly trapped as the cations undergo SCO. The change is the most marked in **2**, consistent with the more abrupt SCO. Interestingly, between 275 and 280 K, **B** and **C** decrease by 0.31 and 0.15 Å and thereafter remain unchanged. This is in the region of the first step in the SCO profile. Upon heating further, **A** decreases by almost 0.2 Å, and as this is the shortest Fe···Fe distance, it correlates with the more abrupt SCO regime. By comparison, in $[Fe(salEen\text{-}I)_2]ClO_4$, the changes in **A**, **B**, and **C** are between 0.14 and 0.61 Å, and even larger than in **2**, resulting in a dramatic explosion of the crystals when they are cooled, following a further shrinking in **A** and **B** independent of SCO activity.[39] Large contractions and expansions in **A**, **B**, and **C** are also observed in $[Fe(salEen\text{-}Br)_2]ClO_4$.[38] In this case, there is a gigantic difference of 2.09 and 1.63 Å in **B** and **C** between the structures at 250 and 300 K, which leads to explosion upon warming above 337 K. The enormous change in the parameters manifests as a coupled

https://doi.org/10.1021/acs.cgd.4c01068
Cryst. Growth Des. 2024, 24, 8145−8152

Table 2. Structural Parameters for Complexes 1 −3

complexes	structural parameter (Å) A	B	C
$[Fe(salEen\text{-}5\text{-}I)_2]Cl$ **1**			
150 K	7.481	9.85	11.26
$[Fe(salEen\text{-}5\text{-}I)_2]Br$ **2**			
123 K	7.970	10.75	11.77
275 K	7.985	10.70	11.75
280 K	7.947	10.39	11.60
293 K	7.773	10.37	11.58
305 K	7.776	10.37	11.58
$[Fe(salEen\text{-}5\text{-}I)_2]I$ **3**			
293 K	8.273	11.33	12.06
400 K	8.239	11.30	11.99
425 K	8.239	11.30	11.99
$[Fe(salEen\text{-}5\text{-}Br)_2]ClO_4$			
250 K (warming)	8.798	14.26	10.30
300 K (cooling)	8.521	12.17	11.93
$[Fe(salEen\text{-}5\text{-}I)_2]ClO_4$			
130 K	8.363	11.43	12.22
150 K	8.394	11.53	12.20
200 K	8.439	11.69	12.18
300 K	8.505	12.04	12.01
350 K	8.480	11.99	11.99
370 K	8.506	12.04	12.02

SCO-thermosalient effect which happens over a small temperature range, resulting in a large hysteretic SCO profile.

In contrast, the changes in compound **3** are more subtle and limited to no more than 0.1 Å. The more compact packing in the latter structure results in a more gradual SCO. The square grid observed in **1**−**3** is also found in many Hoffmann SCO networks in which modeling suggests that subtle differences in the ratio of the nearest and next nearest neighbor contacts can result in the appearance of stepped, hysteretic, and more complex SCO phenomena.[55−57] While the complexes here are held together by supramolecular interactions, it appears that similar rules apply to **1**−**3** and the previously reported and closely related compounds.[58−62]

To date, the impact that anions have on SCO properties remains problematic largely because anions have so many different shapes and sizes.[52] Spherical anions like halides differ only in size and their intermolecular distances, making them the best-studied systems. In most cases, the smaller anion will create a more compact packing and favor the LS state. For example, in $[Fe(trim)_2](halide)_2$ (trim = 4-(4-imidazolylmethyl)-2-(2-imidazolylmethyl)imidazole), the size of the halide modifies the ligand field through imidazole N−H···halide interaction distances and modulates the $T_{1/2}$ of each compound.[63] A similar trend is noted in [Fe(4-OH-sal-*N*-1,4,7,10)]halide[50] and $[Fe(atrz)_3](halide)_2$[51] with $T_{1/2}$ in the order of chloride, bromide, and iodide, respectively. This trend has also been found in $[Fe(qsal\text{-}4\text{-}F)_2]$anion[64] and $[Fe(qsal\text{-}3,5\text{-}Cl)_2]$anion,[65] which include nonspherical counterions. While our compounds broadly follow this trend, the chloride system becomes trapped in the HS state, while the iodide compound exhibits a rather gradual SCO. The more abrupt SCO in **2** seems to rely on a degree of complementarity in the size of the bromide anion with the lattice site which enables a more effective transition of the spin state change.

CONCLUSIONS

In this work, we report three isostructural Fe(III) complexes, $[Fe(salEen\text{-}5\text{-}I)_2]$halide **1**−**3**. The lack of any lattice solvent allows direct comparison between the complexes where we observe that larger anions increasingly favor the LS state. Intriguingly, $[Fe(salEen\text{-}5\text{-}I)_2]Br$ exhibits a stepped SCO that is close to room temperature. Structural studies reveal that a combination of N−H···anion and C−H···anion interactions connect the cations into 2D rhomboidal sheets. The use of structural parameters to describe the nearest and next nearest neighbor contacts allows us to rationalize not only the abruptness of spin crossover but also the stepped nature of the SCO in **2**.[56,57] This is supported by comparisons with previously reported compounds[38,39] and may suggest a way to improve the SCO characteristics in this family by careful crystal engineering.

ASSOCIATED CONTENT

Supporting Information

The Supporting Information is available free of charge at https://pubs.acs.org/doi/10.1021/acs.cgd.4c01068.

Fourier-transform IR (FT-IR) and UV−vis spectroscopic data, electrospray ionisation-mass spectrometry (ESI-MS) data and PXRD plots (PDF)

Accession Codes

CCDC 2374748−2374756 contains the supplementary crystallographic data for this paper. These data can be obtained free of charge via www.ccdc.cam.ac.uk/data_request/cif, by emailing data_request@ccdc.cam.ac.uk, or by contacting The Cambridge Crystallographic Data Centre, 12 Union Road, Cambridge CB2 1EZ, U.K.; fax: +44 1223 336033.

AUTHOR INFORMATION

Corresponding Authors

Phimphaka Harding − *School of Chemistry, Institute of Science, Suranaree University of Technology, Nakhon Ratchasima 30000, Thailand*; Email: phimphaka@g.sut.ac.th

David J. Harding − *School of Chemistry, Institute of Science, Suranaree University of Technology, Nakhon Ratchasima 30000, Thailand*; orcid.org/0000-0001-8866-2401; Email: david@g.sut.ac.th

Authors

Theerapoom Boonprab − *School of Chemistry, Institute of Science, Suranaree University of Technology, Nakhon Ratchasima 30000, Thailand*

Warisa Thammasangwan − *Functional Materials and Nanotechnology Centre of Excellence, Walailak University, Nakhon Si Thammarat 80160, Thailand*

Guillaume Chastanet − *Université de Bordeaux, CNRS, Bordeaux INP, ICMCB, UMR5026, F-33608 Pessac, France*; orcid.org/0000-0001-6829-4066

Mathieu Gonidec − *Université de Bordeaux, CNRS, Bordeaux INP, ICMCB, UMR5026, F-33608 Pessac, France*

Complete contact information is available at: https://pubs.acs.org/10.1021/acs.cgd.4c01068

Author Contributions

‖T.B. and W.T. contributed equally to the work. T.B.: Investigation, formal analysis, data curation, visualization,

https://doi.org/10.1021/acs.cgd.4c01068
Cryst. Growth Des. 2024, 24, 8145−8152

writing—original draft. W.T.: Investigation, formal analysis, data curation. G.C. and M.G.: Investigation, formal analysis, data curation, writing—review and editing. P.H.: Conceptualization, resources, writing—review and editing, supervision, funding acquisition. and D.J.H.: Conceptualization, resources, writing—review and editing, supervision, and funding acquisition.

Notes

The authors declare no competing financial interest.

■ ACKNOWLEDGMENTS

This research has received funding support from the NSRF *via* the Program Management Unit for Human Resources & Institutional Development, Research and Innovation (grant number: B13F670064). We gratefully acknowledge Suranaree University of Technology for partial financial support through the Molecular Magnetic Materials Research Unit.

■ REFERENCES

(1) Murray, K. S. Advances in Polynuclear Iron(II), Iron(III) and Cobalt (II) Spin-Crossover Compounds. *Eur. J. Inorg. Chem.* **2008**, *2008*, 3101−3121.
(2) Halcrow, M. A. *Spin-Crossover Materials: Properties and Applications*; John Wiley & Sons, Ltd., 2013.
(3) Sim, P. G.; Sinn, E. First Manganese(III) Spin Crossover and First d^4 Crossover. Comment on Cytochrome Oxidase. *J. Am. Chem. Soc.* **1981**, *103*, 241−243.
(4) Garcia, Y.; Gütlich, P.Thermal Spin Crossover in Mn(II), Mn(III), Cr(II) and Co(III) Coordination Compounds. In *Topics in Current Chemistry*; Springer, 2004; Vol. *234*, pp 49−62.
(5) Sirirak, J.; Harding, D. J.; Harding, P.; Murray, K. S.; Moubaraki, B.; Liu, L.; Telfer, S. G. Spin Crossover in *cis* Manganese(III) quinolylsalicylaldiminates. *Eur. J. Inorg. Chem.* **2015**, *2015*, 2534−2542.
(6) Gütlich, P.; Garcia, Y.; Goodwin, H. A. Spin crossover phenomena in Fe(II) complexes. *Chem. Soc. Rev.* **2000**, *29*, 419−427.
(7) Gaspar, A. B.; Seredyuk, M.; Gütlich, P. Spin crossover in iron(II) complexes: Recent advances. *J. Mol. Struct.* **2009**, *924*−*926*, 9−19.
(8) Nihei, M.; Shiga, T.; Maeda, Y.; Oshio, H. Spin crossover iron(III) complexes. *Coord. Chem. Rev.* **2007**, *251*, 2606−2621.
(9) Harding, D. J.; Harding, P.; Phonsri, W. Spin Crossover in Iron(III) Complexes. *Coord. Chem. Rev.* **2016**, *313*, 38−61.
(10) Nakanishi, T.; Hori, Y.; Wu, S.; Sato, H.; Okazawa, A.; Kojima, N.; Horie, Y.; Okajima, H.; Sakamoto, A.; Shiota, Y.; Yoshizawa, K.; Sato, O. Three-Step Spin State Transition and Hysteretic Proton Transfer in the Crystal of an Iron(II) Hydrazone Complex. *Angew. Chem., Int. Ed.* **2020**, *59*, 14781−14787.
(11) Li, J.; Wu, S.; Su, S.; Kanegawa, S.; Sato, O. Manipulating Slow Magnetic Relaxation by Light in a Charge Transfer $\{Fe_2Co\}$ Complex. *Chem. - Eur. J.* **2020**, *26*, 3259−3263.
(12) Brooker, S.; Plieger, P. G.; Moubaraki, B.; Murray, K. S. $[Co_2^{II}L(NCS)_2(SCN)_2]$: The First Cobalt Complex to Exhibit Both Exchange Coupling and Spin Crossover Effects. *Angew. Chem., Int. Ed.* **1999**, *38*, 408−410.
(13) Hayami, S.; Komatsu, Y.; Shimizu, T.; Kamihata, H.; Lee, Y. H. Spin-crossover in cobalt(II) compounds containing terpyridine and its derivatives. *Coord. Chem. Rev.* **2011**, *255*, 1981−1990.
(14) Phukkaphan, N.; Cruickshank, D. L.; Murray, K. S.; Phonsri, W.; Harding, P.; Harding, D. J. Hysteretic spin crossover driven by anion conformational change. *Chem. Commun.* **2017**, *53*, 9801−9804.
(15) Karuppannan, S. K.; Martín-Rodríguez, A.; Ruiz, E.; Harding, P.; Harding, D. J.; Yu, X.; Tadich, A.; Cowie, B.; Qi, D.; Nijhuis, C. A. Room temperature conductance switching in a molecular iron(III) spin crossover junction. *Chem. Sci.* **2021**, *12*, 2381−2388.
(16) Hayami, S.; Gu, Z. Z.; Yoshiki, H.; Fujishima, A.; Sato, O. Iron(III) Spin-Crossover Compounds with a Wide Apparent Thermal Hysteresis around Room Temperature. *J. Am. Chem. Soc.* **2001**, *123*, 11644−11650.
(17) Hayami, S.; Hiki, K.; Kawahara, T.; Maeda, Y.; Urakami, D.; Inoue, K.; Ohama, M.; Kawata, S.; Sato, O. Photo-Induced Spin Transition of Iron(III) Compounds with π-π Intermolecular Interactions. *Chem. - Eur. J.* **2009**, *15*, 3497−3508.
(18) Shimizu, T.; Komatsu, Y.; Kamihata, H.; Lee, Y. H.; Fuyuhiro, A.; Iijima, S.; Hayami, S. Photo-switchable spin-crossover iron(III) compound based on intermolecular interactions. *J. Inclusion Phenom. Macrocyclic Chem.* **2011**, *71*, 363−369.
(19) Hayami, S.; Kawahara, T.; Juhász, G.; Kawamura, K.; Uehashi, K.; Sato, O.; Maeda, Y. Iron(III) spin transition compound with a large thermal hysteresis. *J. Radioanal. Nucl. Chem.* **2003**, *255*, 443−447.
(20) Hayami, S.; Gu, Z. Z.; Shiro, M.; Einaga, Y.; Fujishima, A.; Sato, O. First Observation of Light-Induced Excited Spin State Trapping for an Iron(III) Complex. *J. Am. Chem. Soc.* **2000**, *122*, 7126−7127.
(21) Chen, F. L.; Sun, Y. C.; Liu, X. L.; Li, G.; Zhang, C. C.; Gao, B. H.; Zhao, Y.; Wang, X. Y. Spin Crossover in $[Fe(qsal\text{-}5\text{-}Br_q)_2]^+$ Complexes with a Quinoline-Substituted Qsal Ligand. *Inorg. Chem.* **2024**, *63*, 8750−8763.
(22) Floquet, S.; Boillot, M. L.; Rivière, E.; Varret, F.; Boukheddaden, K.; Morineau, D.; Négrier, P. Spin transition with a large thermal hysteresis near room temperature in a water solvate of an iron(III) thiosemicarbazone complex. *New J. Chem.* **2003**, *27*, 341−348.
(23) Kang, S.; Shiota, Y.; Kariyazaki, A.; Kanegawa, S.; Yoshizawa, K.; Sato, O. Heterometallic Fe^{III}/K Coordination Polymer with a Wide Thermal Hysteretic Spin Transition at Room Temperature. *Chem. - Eur. J.* **2016**, *22*, 532−538.
(24) Li, Z. Y.; Dai, J. W.; Gagnon, K. J.; Cai, H. L.; Yamamoto, T.; Einaga, Y.; Zhao, H. H.; Kanegawa, S.; Sato, O.; Dunbar, K. R.; Xiong, R. G. A neutral Fe(III) compound exhibiting a two-step spin transition and dielectric anomalies. *Dalton Trans.* **2013**, *42*, 14685−14688.
(25) Wu, Y. Y.; Li, Z. Y.; Peng, S.; Zhang, Z. Y.; Cheng, H. M.; Su, H.; Hou, W. Q.; Yang, F. L.; Wu, S. Q.; Sato, O.; Dai, J. W.; Li, W.; Bu, X. H. Two-Dimensional Spin-Crossover Molecular Solid Solutions with Tunable Transition Temperatures across 90 K. *J. Am. Chem. Soc.* **2024**, *146*, 8206−8215.
(26) Wu, Y.; Peng, S.; Zhang, Z.; Gao, Y.; Xu, G.; Dai, J.; Li, Z. Y.; Yamashita, M. Controlling Three-Step and Five-Step Spin Transitions by Polymorphism in an Fe^{III} Spin Crossover Complex. *Chin. J. Chem.* **2024**, *42*, 879−886.
(27) Li, Z. Y.; Wu, Y. Y.; Li, Y.; Wang, J. H.; Sulaiman, A.; Javed, M. K.; Zhang, Y. C.; Li, W.; Bu, X. H. Slow Phase Transition-Induced Scan Rate Dependence of Spin Crossover in a Two-Dimensional Supramolecular Fe(III) Complex. *CCS Chem.* **2023**, *5*, 412−422.
(28) Li, Z. Y.; Ohtsu, H.; Kojima, T.; Dai, J. W.; Yoshida, T.; Breedlove, B. K.; Zhang, W. X.; Iguchi, H.; Sato, O.; Kawano, M.; Yamashita, M. Direct Observation of Ordered High-Spin-Low-Spin Intermediate States of an Iron(III) Three-Step Spin-Crossover Complex. *Angew. Chem., Int. Ed.* **2016**, *55*, 5184−5189.
(29) Sheu, C. F.; Chen, S. M.; Lee, G. H.; Liu, Y. H.; Wen, Y. S.; Lee, J. J.; Chuang, Y. C.; Wang, Y. Structure and Magnetism of the Iron(III) Spin-Crossover Complex $[Fe^{III}\{N\text{-ethyl-}N\text{-(2-aminoethyl)-salicylaldiminate}\}_2]ClO_4$. *Eur. J. Inorg. Chem.* **2013**, *2013*, 894−901.
(30) Tissot, A.; Fertey, P.; Guillot, R.; Briois, V.; Boillot, M. L. Structural, Magnetic, and Vibrational Investigations of Fe^{III} Spin-Crossover Compounds $[Fe(4\text{-MeO-SalEen})_2]X$ with X = NO_3^- and PF_6^-. *Eur. J. Inorg. Chem.* **2014**, *2014*, 101−109.
(31) Martinho, P. N.; Vicente, A. I.; Realista, S.; Saraiva, M. S.; Melato, A. I.; Brandão, P.; Ferreira, L. P.; de Deus Carvalho, M. Solution and solid state properties of Fe(III) complexes bearing *N*-ethyl-*N*-(2-aminoethyl)salicylaldiminate ligands. *J. Organomet. Chem.* **2014**, *760*, 48−54.
(32) Gruzdev, M.; Chervonova, U.; Vorobeva, V. The Branched Schiff Base Cationic Complexes of Iron(III) with Different Counter-Ions. *Symmetry* **2022**, *14*, No. 1140.

https://doi.org/10.1021/acs.cgd.4c01068
Cryst. Growth Des. 2024, 24, 8145−8152

(33) Dey, B.; Gupta, A.; Kapurwan, S.; Konar, S. Study of Spin Crossover Property of a Series of X-OMe-SalEen (X = 6, 5 and 4) Based Fe(III) Complexes. *ChemistrySelect* **2020**, *5*, 14677−14684.
(34) Dey, B.; Mehta, S.; Mondal, A.; Cirera, J.; Colacio, E.; Chandrasekhar, V. Push and Pull Effect of Methoxy and Nitro Groups Modifies the Spin-State Switching Temperature in Fe(III) Complexes. *ACS Omega* **2022**, *7*, 39268−39279.
(35) Dey, B.; Cirera, J.; Mehta, S.; Ferreira, L. P.; Arumugam, R.; Mondal, A.; Martinho, P. N.; Chandrasekhar, V. Steric Effects on Spin States in a Series of Fe(III) Complexes. *Cryst. Growth Des.* **2023**, *23*, 6668−6678.
(36) Haddad, M. S.; Federer, W. D.; Lynch, M. W.; Hendrickson, D. N. An Explanation of Unusual Properties of Spin-Crossover Ferric Complexes. *J. Am. Chem. Soc.* **1980**, *102*, 1468−1470.
(37) Haddad, M. S.; Federer, W. D.; Lynch, M. W.; Hendrickson, D. N. Spin-Crossover Ferric Complexes: Unusual Effects of Grinding and Doping Solids. *Inorg. Chem.* **1981**, *20*, 131−139.
(38) Vicente, A. I.; Joseph, A.; Ferreira, L. P.; De Deus Carvalho, M.; Rodrigues, V. H. N.; Duttine, M.; Diogo, H. P.; Da Piedade, M. E. M.; Calhorda, M. J.; Martinho, P. N. Dynamic spin interchange in a tridentate Fe(III) Schiff-base compound. *Chem. Sci.* **2016**, *7*, 4251−4258.
(39) Martins, F. F.; Joseph, A.; Diogo, H. P.; da Piedade, M. E. M.; Ferreira, L. P.; Carvalho, M. D.; Barroso, S.; Romão, M. J.; Calhorda, M. J.; Martinho, P. N. Irreversible magnetic behaviour caused by the thermosalient phenomenon in an iron(III) spin crossover complex. *Eur. J. Inorg. Chem.* **2018**, *2018*, 2976−2983.
(40) Bento, M. A.; Gomes, T.; Martins, F. F.; Gil, A.; Ferreira, L. P.; Barroso, S.; Gomes, C. S. B.; Garcia, Y.; Martinho, P. N. The role of intermolecular interactions in $[Fe(X\text{-}salEen)_2]ClO_4$ spin crossover complexes. *Dalton Trans.* **2024**, *53*, 8791−8802.
(41) Boonprab, T.; Harding, P.; Murray, K. S.; Phonsri, W.; Telfer, S. G.; Alkaş, A.; Ketkaew, R.; Tantirungrotechai, Y.; Jameson, G. N. L.; Harding, D. J. Solvatomorphism and anion effects in predominantly low spin iron(III) Schiff base complexes. *Dalton Trans.* **2018**, *47*, 12449−12458.
(42) Boonprab, T.; Lee, S. J.; Telfer, S. G.; Murray, K. S.; Phonsri, W.; Chastanet, G.; Collet, E.; Trzop, E.; Jameson, G. N. L.; Harding, P.; Harding, D. J. The First Observation of Hidden Hysteresis in an Iron(III) Spin-Crossover Complex. *Angew. Chem., Int. Ed.* **2019**, *58*, 11811−11815.
(43) Al-Azzani, M. A.; Al-Mjeni, F.; Mitsuhashi, R.; Mikuriya, M.; Al-Omari, I. A.; Robertson, C. C.; Bill, E.; Shongwe, M. S. Unusual Magneto-Structural Features of the Halo-Substituted Materials $[Fe^{III}(5\text{-}X\text{-}salMeen)_2]Y$: a Cooperative [HS-HS]↔[HS-LS] Spin Transition. *Chem. - Eur. J.* **2020**, *26*, 4766−4779.
(44) Petty, R. H.; Dose, E. V.; Tweedle, M. F.; Wilson, L. J. Bis(*N*-methylethylenediaminesalicylaldiminato) iron(III) Complexes. Magnetic, Mössbauer, and Intersystem Crossing Rate Studies in the Solid and Solution States for a New (S = 1/2)↔(S = 5/2) Spin-Equilibrium Case. *Inorg. Chem.* **1978**, *17*, 1064−1071.
(45) Ketkaew, R.; Tantirungrotechai, Y.; Harding, P.; Chastanet, G.; Guionneau, P.; Marchivie, M.; Harding, D. J. OctaDist: a tool for calculating distortion parameters in spin crossover and coordination complexes. *Dalton Trans.* **2021**, *50*, 1086−1096.
(46) Boonprab, T.; Habarakada, U.; Chastanet, G.; Harding, P.; Harding, D. J. Light and thermally activated spin crossover coupled to an order-disorder transition of a propyl chain in an iron(III) complex. *CrystEngComm* **2023**, *25*, 4126−4132.
(47) Vicente, A. I.; Ferreira, L. P.; Carvalho, M. D.; Rodrigues, V. H. N.; Dîrtu, M. M.; Garcia, Y.; Calhorda, M. J.; Martinho, P. N. Selecting the spin crossover profile with controlled crystallization of mononuclear Fe(III) polymorphs. *Dalton Trans.* **2018**, *47*, 7013−7019.
(48) Nemec, I.; Kotásková, L.; Herchel, R. Variation of Spin-Transition Temperature in the Iron(III) Complex Induced by Different Compositions of the Crystallization Solvent. *Cryst. Growth Des.* **2023**, *23*, 1323−1329.
(49) Marques, R. T.; Ferreira, L. P.; Gomes, C. S. B.; Lopes, C. S. D.; Bernardes, C. E. S.; Sarangi, N. K.; Keyes, T. E.; Martinho, P. N. Reversible Single-Crystal-to-Single-Crystal Transformations in a salEen Fe(III) Spin Crossover Sponge. *Cryst. Growth Des.* **2023**, *23*, 3222−3229.
(50) Nemec, I.; Herchel, R.; Šalitroš, I.; Trávníček, Z.; Moncoľ, J.; Fuess, H.; Ruben, M.; Linert, W. Anion driven modulation of magnetic intermolecular interactions and spin crossover properties in an isomorphous series of mononuclear iron(III) complexes with a hexadentate Schiff base ligand. *CrystEngComm* **2012**, *14*, 7015−7024.
(51) Askew, J. H.; Shepherd, H. J. Post-synthetic Anion Exchange in iron(II) 1,2,4-Triazole Based Spin Crossover Materials *via* Mechanochemistry. *Dalton Trans.* **2020**, *49*, 2966−2971.
(52) Zhao, S.-Z.; Zhou, H.-W.; Qin, C.-Y.; Zhang, H.-Z.; Li, Y.-H.; Yamashita, M.; Wang, S. Anion Effects on Spin Crossover Systems: From Supramolecular Chemistry to Magnetism. *Chem. - Eur. J.* **2023**, *29*, No. e202300554.
(53) Cavallo, G.; Biella, S.; Lü, J.; Metrangolo, P.; Pilati, T.; Resnati, G.; Terraneo, G. Halide anion-templated assembly of di- and triiodoperfluorobenzenes into 2D and 3D supramolecular networks. *J. Fluorine Chem.* **2010**, *131*, 1165−1172.
(54) Pfrunder, M. C.; Brock, A. J.; Micallef, A. S.; Clegg, J. K.; McMurtrie, J. Halogen-Bond-Modulated Organization of $[Ni(terpy\text{-}ph)_2]I_2$ Complexes in Heteromeric Three-Component Systems. *Cryst. Growth Des.* **2019**, *19*, 5334−5342.
(55) Singh, Y.; Oubouchou, H.; Nishino, M.; Miyashita, S.; Boukheddaden, K. Elastic-frustration-driven unusual magnetoelastic properties in a switchable core-shell spin-crossover nanostructure. *Phys. Rev. B* **2020**, *101*, No. 054105.
(56) Cruddas, J.; Powell, B. J. Structure-property relationships and the mechanisms of multistep transitions in spin crossover materials and frameworks. *Inorg. Chem. Front.* **2020**, *7*, 4424−4437.
(57) Ndiaye, M.; Singh, Y.; Fourati, H.; Sy, M.; Lo, B.; Boukheddaden, K. Isomorphism between the electro-elastic modeling of the spin transition and Ising-like model with competing interactions: Elastic generation of self-organized spin states. *J. Appl. Phys.* **2021**, *129*, No. 153901.
(58) Paez-Espejo, M.; Sy, M.; Boukheddaden, K. Elastic Frustration Causing Two-Step and Multistep Transitions in Spin-Crossover Solids: Emergence of Complex Antiferroelastic Structures. *J. Am. Chem. Soc.* **2016**, *138*, 3202−3210.
(59) Paez-Espejo, M.; Sy, M.; Boukheddaden, K. Unprecedented Bistability in Spin-Crossover Solids Based on the Retroaction of the High Spin Low-Spin Interface with the Crystal Bending. *J. Am. Chem. Soc.* **2018**, *140*, 11954−11964.
(60) Azzolina, G.; Bertoni, R.; Collet, E. General Landau theory of non-symmetry-breaking and symmetry-breaking spin transition materials. *J. Appl. Phys.* **2021**, *129*, No. 085106.
(61) Collet, E.; Azzolina, G. Coupling and decoupling of spin crossover and ferroelastic distortion: Unsymmetric hysteresis loop, phase diagram, and sequence of phases. *Phys. Rev. Mater.* **2021**, *5*, No. 044401.
(62) Nadeem, M.; Cruddas, J.; Ruzzi, G.; Powell, B. J. Toward High-Temperature Light-Induced Spin-State Trapping in Spin-Crossover Materials: The Interplay of Collective and Molecular Effects. *J. Am. Chem. Soc.* **2022**, *144*, 9138−9148.
(63) Lemercier, G.; Bréfuel, N.; Shova, S.; Wolny, J. A.; Dahan, F.; Verelst, M.; Paulsen, H.; Trautwein, A. X.; Tuchagues, J. P. A Range of Spin-Crossover Temperature $T_{1/2}$ > 300 K Results from Out-of-Sphere Anion Exchange in a Series of Ferrous Materials Based on the 4-(4-imidazolylmethyl)-2-(2-imidazolylmethyl)imidazole (trim) ligand, $[Fe(trim)_2]X_2$ (X = F, Cl, Br, I): Comparison of Experimental Results with Those Derived from Density Functional Theory Calculations. *Chem. - Eur. J.* **2006**, *12*, 7421−7432.
(64) Sheng, H. J.; Xia, C. C.; Zhang, X. Y.; Zhang, C. C.; Ji, W. J.; Zhao, Y.; Wang, X. Y. Anion Modified Spin Crossover in $[Fe(qsal\text{-}4\text{-}F)]^+$ Complexes with a 4-Position Substituted Qsal Ligand. *Inorg. Chem.* **2022**, *61*, 12726−12735.

https://doi.org/10.1021/acs.cgd.4c01068
Cryst. Growth Des. 2024, 24, 8145−8152

(65) Jeong, A. R.; Park, S. R.; Shin, J. W.; Kim, J.; Tokunaga, R.; Hayami, S.; Min, K. S. Mononuclear Fe(III) complexes with 2,4-dichloro-6-((quinoline-8-ylimino)methyl)phenolate: synthesis, structure, and magnetic behavior. *Dalton Trans.* **2024**, *53*, 6809−6817.

https://doi.org/10.1021/acs.cgd.4c01068
Cryst. Growth Des. 2024, 24, 8145−8152